Stellar Atmosphere Modelling
ASP Conference Series, Vol. ?, 2002
I. Hubeny, D. Mihalas, & K. Werner

Basic ALI in Moving Atmospheres

Wolf-Rainer Hamann
Astrophysik, Universität Potsdam, Am Neuen Palais 10, D-14469 Potsdam, Germany

Abstract. The non-LTE radiative transfer problem requires the consistent solution of two sets of equations: the radiative transfer equations, which couple the spatial points, and the equations of the statistical equilibrium, which couple the frequencies. The "Accelerated Lambda Iteration" (ALI) method allows for an iterative scheme, in which both sets of equations are solved in turn.

For moving atmospheres the radiative transfer is preferably formulated in the co-moving frame-of-reference, which leads to a partial differential equation. "Classical" numerical solution methods are based on differencing schemes. For better numerical stability, we prefer "short characteristics" integration methods.

Iron line blanketing is accounted for by means of the "superlevel" concept. In contrast to static atmospheres, the frequencies can not be re-ordered in the moving case because of the frequency coupling from Doppler shifts.

One of our future aims is the coupling of elaborated radiative transfer calculations with the hydrodynamical equations in order to understand the driving of strong stellar winds, especially from Wolf-Rayet stars.

1. Accelerated Lambda Iteration

Astrophysical plasmas are often far from being in Local Thermodynamical Equilibrium (LTE). This holds especially for the expanding atmospheres of hot stars. The general concept of "Accelerated Lambda Iteration" (ALI) techniques, which will be outlined below in this section, allows to handle such non-LTE problems. The radiative transfer in stellar winds is to be solved in the Co-Moving Frame of reference, and Approximate Lambda Operators (ALOs) must be adapted to the moving case. In Sect. 2 we briefly describe our code for expanding atmospheres, present some examples of Wolf-Rayet models, and discuss the wind driving mechanism.

1.1. The Non-LTE Problem

The Radiative Transfer Equation couples the different spatial points of the stellar atmosphere. It is usually written as a differential equation. More general, it might be considered as a linear mapping $\mathbf{\Lambda}$ between two functions of the spatial coordinates and the frequency: the (angle-averaged) radiation field $\mathbf{J}$, and the source function $\mathbf{S}$, symbolically

$$\mathbf{J}_{\mathrm{fs}} = \mathbf{\Lambda}\,\mathbf{S}(\mathbf{n}) \ . \tag{1}$$

The source function depends on the full set set of population numbers (all atomic levels) n at that spatial point. If the source function is given, we speak of a "formal solution" (fs) of the transfer problem. The transfer equations for different frequency point are not coupled, as long as formal solutions in static media are considered.

However, in the non-LTE case the population numbers n depend from the radiation field. Assuming stationarity, the gains and losses of each atomic level must be statistically balanced. This means that at each spatial point, the set of population numbers (written as a row vector $\vec{n}$) has to be calculated from the "Rate Equations" (equations of statistical equilibrium),

$$\vec{n} \circ \mathbf{P}(\mathbf{J}) = [\mathbf{0}, ..., \mathbf{0}, \mathbf{1}] \ . \tag{2}$$

The coefficient matrix $\mathbf{P} = \mathbf{C} + \mathbf{R}$ describes the transition probabilities between the atomic levels by collisional ($\mathbf{C}$) and radiative ($\mathbf{R}$) processes. The latter have the form of *frequency* integrals over the cross section $\sigma(\nu)$ times radiation intensity J_ν, e.g.

$$R_{lu} = \int \frac{4\pi}{h\nu}\ \sigma_{lu}(\nu)\ J_\nu\ \mathrm{d}\nu \ . \tag{3}$$

By those integrals, the radiation field at *all frequencies* is (non-linearly) involved in the rate equations.

The extreme difficulty in solving non-LTE problems is due to the need for solving *consistently* these two sets of equations described above: the Radiative Transfer Equations which couple the spatial points, and the Rate Equations which couple the frequencies.

1.2. Accelerated Lambda Iteration (ALI)

A simple strategy for solving the non-LTE problem is called "Lambda Iteration". Starting from a set of "old" population numbers, the radiative transfer is calculated. Then the obtained "formal solution" is taken as "new" radiation field, i.e. as input for solving the Rate Equations, formally:

$$\mathbf{J}_{\mathrm{fs}} = \mathbf{\Lambda}\,\mathbf{S}(\mathbf{n}_{\mathrm{old}}) \ ; \quad \mathbf{J}_{\mathrm{new}} = \mathbf{J}_{\mathrm{fs}} \ ; \quad \mathbf{n}_{\mathrm{new}} \circ \mathbf{P}(\mathbf{J}_{\mathrm{new}}) = [\mathbf{0}, ..., \mathbf{0}, \mathbf{1}] \ . \tag{4}$$

The "new" population numbers enter the next iteration cycle as n_{old}. However, it is known since long that such an iterative procedure fails to converge if there are optically thick transitions, i.e. in most cases of practical interest.

As a major breakthrough, it was discovered in the 1980s that convergence of that simple scheme can be retained even for optically thick cases (see e.g. Werner & Husfeld 1985, Hamann 1985, 1986). To achieve this, the middle step of Eq. (4), $\mathbf{J}_{\mathrm{new}} = \mathbf{J}_{\mathrm{fs}}$, is replaced by

$$\mathbf{J}_{\mathrm{new}} = \mathbf{J}_{\mathrm{fs}} \ + \ \mathbf{\Lambda}^{*}[\mathbf{S}(\mathbf{n}_{\mathrm{new}}) - \mathbf{S}(\mathbf{n}_{\mathrm{old}})] \ . \tag{5}$$

Here $\mathbf{\Lambda}^{*}$ denotes a so-called *Approximate Lambda Operator* (ALO). It can be chosen sufficiently simple for being incorporated into the Rate Equations, but must be accurate enough for large optical depth. As for large opacities most photons are locally trapped, even a local ("diagonal") $\mathbf{\Lambda}^*$ can be sufficient (cf. Sect. 1.5).

By inserting Eq. (5) into the rate equations, the coefficient matrix $\mathbf{P}$ becomes explicitely dependent on the yet unknown population numbers $\mathbf{n}_{\rm new}$. Hence the Rate Eqs. become *non-linear* in n, and adequate methods should be applied for their efficient and accurate solution (e.g. Koesterke, Hamann, & Kosmol 1992).

1.3. Radiative transfer in the Co-Moving Frame (angle-dependent)

The radiative transfer in moving media is preferably formulated in the Co-Moving Frame of reference (CMF) (Fig. 1). The CMF transfer equation for the specific intensity I at (dimensionless) CMF frequency x and spatial coordinate z becomes

$$\pm \frac{\partial I^\pm}{\partial z} - P \frac{\partial I^\pm}{\partial x} = \eta - \kappa I^\pm \tag{6}$$

for rays propagating in $+z$ and $-z$ direction, respectively. P is the velocity gradient (in appropriate dimensionless units) projected on that ray. Thus, by transformation into the CMF, the transfer equation becomes a *partial* differential equation for the intensity I.

Solution with differencing scheme. The standard technique for solving the above angle-dependent ("ray-by-ray") transfer equation was formulated by Mihalas, Kunasz, & Hummer (1975). As for the static case, one defines the "Feautrier variables"

$$u = \frac{1}{2}(I^+ + I^-) \qquad v = \frac{1}{2}(I^+ - I^-) \tag{7}$$

and obtains two coupled partial differential equations for u and v. But unlike the static case, v cannot be eliminated by inserting one equation into the other. Instead, both PDEs are discretized on a mesh in space and frequency. The differencing scheme, of second order in space and of first order in frequency, yields

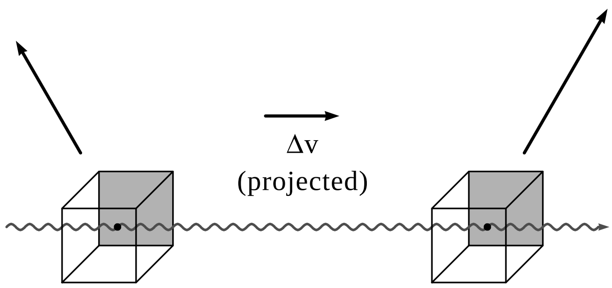

Figure 1. In a spherically-expanding atmosphere with accelerated outflow, any two volume elements are receding from each other. The frequency of a traveling photon, when measured in the co-moving frame-of-reference of each volume element, thus experiences a redshift according to the velocity difference projected on that ray.

an algebraic system which can be solved frequency after frequency, proceeding from the blue to the red.

In the practical application of that method, instabilities are sometimes encountered when two adjacent $\Delta\tau$ steps are too different. As a more severe problem, negative intensities often occur at the red wing of strong emission lines (Fig. 2). This is fatal when those resulting intensities shall be used to calculate "Eddington factors" for the Moment Equations (see below).

Solution with Short Characteristics Integration This technique, which overcomes the just mentioned problems of the differencing schemes, has been described for the the ray-by-ray CMF transfer by Koesterke, Hamann & Gräfener (2002). After introducing a mesh in space (z_l) and frequency (x_k), the integration is carried out along the characteristics across each cell (cf. Fig. 3). Along its characteristic, the *partial* differential equation transforms to an *ordinary* differential equation, which here is just the transfer equation in the observer's frame. Defining the source function S and the optical depth τ along the ray in the usual way, one obtains

$$I^+_{l,k} = \int_{\tau=0}^{\hat{\tau}} S(\tau)\ e^{-\tau} d\tau \ + \ \hat{I}^+ e^{-\hat{\tau}} \qquad (8)$$

which can be calculated as an quadrature sum

$$I^+_{l,k} = w_0 S_{l,k} \ + \ \hat{w}\hat{S} \ + \ \hat{I}^+ e^{-\hat{\tau}} \ \text{ with } \ w_0 = 1 - \frac{1-e^{-\hat{\tau}}}{\hat{\tau}}\ , \ \ \hat{w} = 1 - w_0 - e^{-\hat{\tau}} \qquad (9)$$

being the weights incorporating the $e^{-\tau}$ factor.

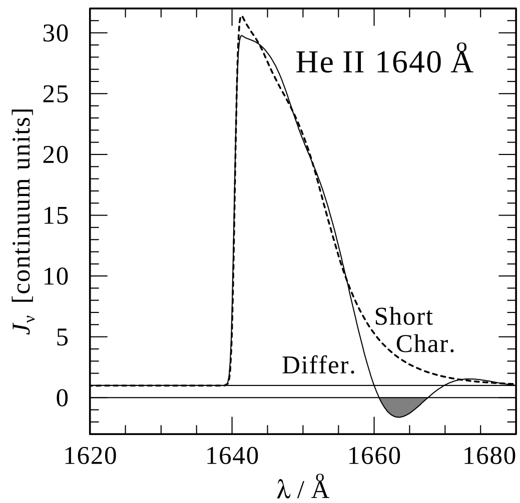

Figure 2. Mean intensities J_ν at some interior point of a test model atmosphere around a strong spectral line. At the red line-wing, the solution obtained from a differencing scheme (solid line) swings below the continuum level and even becomes negative (grey area). In contrast, the Short-Characteristics integration (dashed line) gives always positive intensities by construction.

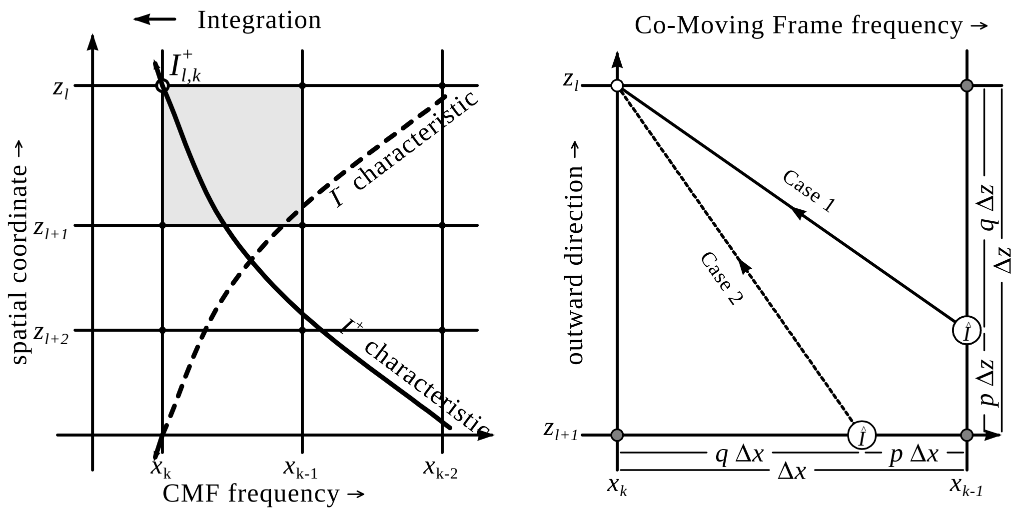

Figure 3. Characteristics of the co-moving frame transfer equation. The left panel shows two "long" characteristics for a ray in outward and inward direction, respectively. In the *short characteristic* method, any characteristic is only followed back to the boundary of the mesh cell. One particular cell (grey in the left panel) is sketched in the right panel in more detail, showing the outward ray which meets the mesh point x_k, z_l. Within the cell the characteristic is approximated by a straight line. The ray enters the cell with intensity $\hat{I}^+$ either across the frequency border (case 1) or across the spatial border (case 2).

At the point where the characteristic enters the mesh cell, the initial value $\hat{I}^+$ is obtained from interpolation. Depending on whether the characteristic crosses the frequency or the spatial boundary of the mesh cell, two cases (1 and 2) must be distinguished. The inward direction (I^-) is treated analogously. When stepping through the grid first down (for I^-) and then up (for I^+) in z_l, for subsequent frequencies x_k, all intensities needed for the interpolation on the cell boundaries are provided in time. Higher-order interpolation is necessary especially at the frequency boundary x_{k-1}.

The short characteristics integration scheme guaranties positive intensities by construction. In the practical application it works stable, while the computational costs are similar as for the differencing methods.

1.4. Radiative transfer in the Co-Moving Frame: Moment Equations

The application of the *Moment Equations* of radiative transfer has two advantages over the ray-by-ray formulation discussed in the previous subsection. First, it is computationally faster than ray-by-ray solutions because the latter have to be done separately for each spatial direction (angle or impact parameter mesh point). Second, coherent scattering (as usually adopted for Thomson scattering) cancels out in the Moment Equations.

The first four *moments* of the radiation field are termed J, H, K, N and defined by the angle integrals

$$J_\nu, H_\nu, K_\nu, N_\nu = \frac{1}{2} \int_{-1}^{1} I_\nu \, \mu^n \, \mathrm{d}\mu \quad \text{for} \quad n = 0, 1, 2, 3 \tag{10}$$

respectively, with $\mu = \cos\theta$. In spherical geometry, it is useful to introduce also "tilded" moments $\tilde{J}_\nu = r^2 J$ and so on. For an atmosphere expanding with the velocity field $v(r)$, the Moment Equations read

$$\frac{\partial \tilde{H}_\nu}{\partial r} - \left(\frac{\mathrm{d}v}{\mathrm{d}r} - \frac{v}{r}\right) \frac{\partial \tilde{K}_\nu}{\partial x} - \frac{v}{r} \frac{\partial \tilde{J}_\nu}{\partial x} = \tilde{\eta}_\nu^{\mathrm{true}} - \kappa^{\mathrm{true}} \tilde{J}_\nu \tag{11}$$

$$\frac{\partial (q \tilde{K}_\nu)}{-q \, \partial r} + \left(\frac{\mathrm{d}v}{\mathrm{d}r} - \frac{v}{r}\right) \frac{\partial \tilde{N}_\nu}{\partial x} + \frac{v}{r} \frac{\partial \tilde{H}_\nu}{\partial x} = \kappa \, \tilde{H}_\nu \tag{12}$$

(refer to Gräfener, Koesterke, & Hamann 2002 for details of this notation). This system of two partial differential equations for the first four moments is closed by means of "Eddington factors", which relate the highest moments (K and N) to the lower moments (J and H). The Eddington factors are updated every, say, six iterations by solving the angle-dependent radiative transfer (cf. preceding subsection).

Those Eddington factors were originally defined (Mihalas, Kunasz, & Hummer 1976) as

$$f_\nu = \frac{K_\nu}{J_\nu} \quad \text{and} \quad g_\nu = \frac{N_\nu}{H_\nu} \; . \tag{13}$$

If the ray-by-ray intensities are calculated with the Short Characteristic method (see above), I_ν and therefore J_ν is always positive and hence f_ν is well-defined. However, in real atmospheres there are always depths and frequencies where flux is directed inwards, i.e. where H_ν can pass through zero and thus g_ν is not well defined. The hyperbolic type of the PDE system is given if $g(\frac{\mathrm{d}v}{\mathrm{d}r} - \frac{v}{r}) + \frac{v}{r} > 0$. Both, a positive denominater and the hyperbolic type, can be achieved by modifying the definition of g_ν to

$$g_\nu = \frac{N_\nu}{H_\nu + \epsilon J_\nu} \tag{14}$$

and chosing a high enough (possibly depth-dependent) value for ϵ.

Solution with differencing scheme. The Moment Equations can be solved by means of a differencing scheme of similar structure as for the ray-by-ray equation (cf. Hillier 1990, Gräfener et al. 2002). After introducing a discrete mesh of radius (r_l) and CMF-frequency (x_k) points, the intensities and fluxes at x_k are arranged in vectors $\vec{J}_k$ and $\vec{H}_k$. After both Moment Equations (Eqs. 11 and 12) are written as difference equations, $\vec{H}_k$ can be eliminated from the first equation by means of the second one, which yields a second-order scheme for $\vec{J}_k$. It involves $\vec{H}_{k-1}$, which are defined on radius interstices. $\vec{H}_k$ is then calculated directly from the discretized Eq. (12) before the integration proceeds to the next frequency index $k{+}1$. In the practical application, the method works satisfactory except of instabilities in cases when $\Delta\tau$ becomes very different for adjacent steps, e.g. where ionization stages are changing abruptly.

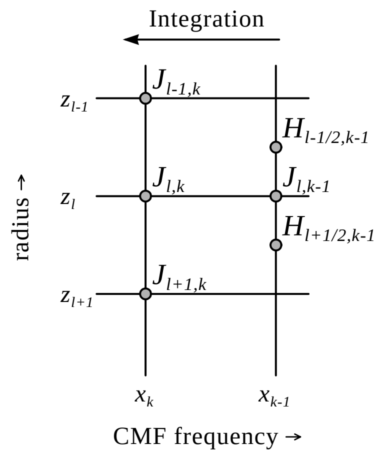

$$\mathbf{T}_k \vec{J}_k = \mathbf{V}_k \vec{H}_{k-1} + \mathbf{U}_k \vec{J}_{k-1} + \vec{S}_k$$

$$\vec{H}_k = \mathbf{A}_k \vec{J}_k + \mathbf{B}_k \vec{H}_{k-1}$$

Figure 4. Differencing scheme for the moment equations in the Co-Moving Frame. Matrix $\mathbf{T}_k$ is tridiagonal, the other coefficient matrices are diagonal or bidiagonal. The sketch illustrates to which other variables $J_{l,k}$ is coupled by the first equation. The second equation is subsequently applied to establish the flux H at the frequency index k for the radius interstices, before the integration proceeds to the next k.

Solution with Short Characteristics Integration Because of the just mentioned instabilities, and motivated by the good experiences in the ray-by-ray cases, we are looking for a Short Characteristics Integration method also for the Moment Equations (Hamann, Friedl, & Feldmeier, in preparation). Recall that the Moment Equations (Eqs. 11 and 12) form a system of Partial Differential Equations of hyperbolic type. Such a system has two real characteristics, which can be found as follows.

Note that both of the PDEs (Eqs. 11 and 12) have the general form

$$\left[a_1 \frac{\partial}{\partial r} + a_2 \frac{\partial}{\partial x}\right] \tilde{J} \; + \; \left[b_1 \frac{\partial}{\partial r} + b_2 \frac{\partial}{\partial x}\right] \tilde{H} \; + \; (...)\tilde{J} \; + \; (...)\tilde{H} = (...) \tag{15}$$

Each of the brackets [...] can be considered as a *directional* derivative. Generally, those derivatives of $\tilde{J}$ and $\tilde{H}$ point in *different* directions. Following the method of “Riemann Invariants”, one can form new equations as a linear combination of the two PDEs, e.g. $\lambda(r, x) \times$ [Eq. (11)] + [Eq. (12)]. There exist two functions λ (λ^+ and λ^-) such that in the new equations *both* derivatives (acting on $\tilde{J}$ and on $\tilde{H}$, respectively) are pointing into the *same* direction, i.e. $\frac{a_1}{a_2} = \frac{b_1}{b_2}$. These two directions are the directions of the two *characteristics* in that point. For an expanding atmosphere they proceed blueward, one in outward (+) and one in inward (−) direction.

Hence, the linear combinations with λ^+ yields a new differential equation which contains only a derivative along its “+” characteristic curve. This is equivalent to an *Ordinary* Differential Equation along that characteristic. The derivative (with respect to some curve parameter) acts effectively on a linear combination of J and H, the so-called “Riemann Invariant” R^+. If chosing the r coordinate as curve parameter, and considering the “−” characteristic in the

$$\frac{\mathrm{d}R^+}{\mathrm{d}\sigma^+} + \alpha^+ R^+ = \gamma^+ R^- + \delta^+$$

$$\frac{\mathrm{d}R^-}{\mathrm{d}\sigma^-} + \alpha^- R^- = \gamma^- R^+ + \delta^-$$

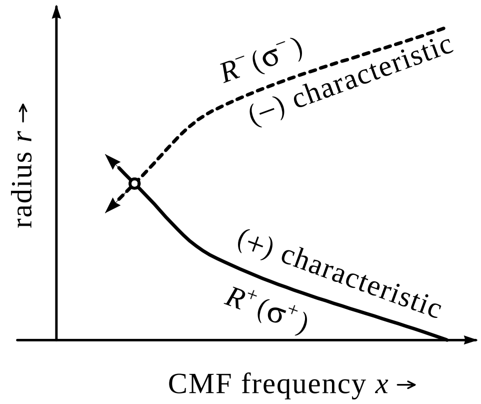

Figure 5. Structure of the Moment Equations in the CMF after transformation to "Riemann invariants" (Eq. 16). For each of the variables there is one Ordinary Differential Equation, each defined on the corresponding characteristic curve (see sketch). Both equations are mutually coupled: at any point of the "+" characteristic, the differential equation for R^+ contains the value of R^- which is delivered there by the intersecting "−" characteristic from the other ODE, and vice versa.

same way, we get

$$R^+ = f\tilde{J} + \lambda^+ \tilde{H} \quad \text{and} \quad R^- = f\tilde{J} + \lambda^- \tilde{H} \ . \tag{16}$$

Note that the two ODEs for R^+ and R^- are defined each on their own characteristic curve (see Fig. 5).

The Short Characteristics integration scheme may be the same as in the ray-by-ray case (cf. Sect. 1.3). However, because of the mutual coupling, the integration cannot be carried out independently for both equations. Instead, at a given frequency index k we collect all coefficients for both Riemann Invariants and arrange them into a 2×2 block matrix scheme, augment this by the usual boundary conditions, and solve this linear system ("Feautrier scheme") by elimination. – It is still to early to assess the final success of this method.

1.5. ALOs for moving atmospheres

Now we turn to the question how "Approximate Lambda Operators" can be constructed for moving atmospheres. Diagonal ALOs might be obtained from the ad-hoc consideration, that the optical depth τ_ν of some point in the atmosphere determines the fraction of locally trapped photons, e.g. for continua: $\Lambda^*_\nu = 1 - \exp(-\tau_\nu/\gamma)$ with some adjustable parameter γ of order unity. For lines, the "core saturation" concept might be adapted to the moving case (Hamann 1985), which means that we set $\Lambda^*_\nu = 1$ in the optically thick line core (if $\tau > \gamma$), and $\Lambda^*_\nu = 0$ in the optically thin line wings. Despite it's naive nature, this type of operator is still optionally used with success in the Potsdam code.

As has been pointed out by Olson, Auer, & Buchler (1986), a nearly optimal diagonal ALO is given by the diagonal of the *exact* lambda operator. Formally, we may identify the diagonal elements of Λ^*_ν with the explicit dependence of $J_{l,k}$ on the source function $S_{l,k}$ at the same frequency- and radius point. The corresponding coefficients can be obtained as a by-product of the radiative transfer calculation.

For instance, when we are solving the CMF transfer ray-by-ray by integration along short characteristics, we have (Eq. 9) $I_{l,k}(\mu) = w_0(\mu)\ S_{l,k} + ...$ and thus, by integrating over angle for obtaining J, one sees that

$$\Lambda^*_{l,k} = \frac{1}{2}\int w_0(\mu)\ \mathrm{d}\mu \tag{17}$$

is the diagonal element of the (approximate) lambda operator.

If we apply the CMF Moment equations represented by a differencing scheme, the tridiagonal system (see Fig. 4) $\mathbf{T}_k\vec{J}_k = \mathbf{V}_k\vec{H}_{k-1} + \mathbf{U}_k\vec{J}_{k-1} + \vec{S}_k$ must be solved for $\vec{J}_k$. The explicit dependence on the source function is obviously given by the diagonal element of the inverse of $\mathbf{T}_k$, i.e. $\Lambda^*_{l,k} = (\mathbf{T}_k^{-1})_{l,l}$.

The method used in the code of Hillier & Miller (1998) is equivalent to a tridiagonal ALO approach. They linearize the transfer equation and evaluate the first-order dependence of the radiation intensity $J_{l,k}$ on the population numbers n_i at the same radius point r_l and the adjacent radius points.

1.6. Inhomogeneous atmospheres ("clumping")

There are various evidences that the expanding atmospheres of hot stars are not homogeneous, but structured on different scales. Density inhomogeneities on small scales (compared to the photon's free path) can be accounted for in a simple approximation. We assume that the density in the clumps is enhanced by a factor $D > 1$, compared to a smooth model with same mass-loss rate. The interclump medium is adopted to be void, i.e. the volume filling factor of the clumps is $f_\mathrm{V} = D^{-1}$. (For simplicity we take D constant over the whole atmosphere.) The radiative transfer is calculated with a spatial average of the emissivities and opacities, while the Rate Equations are solved for the enhanced density in the clumps.

The emission lines from dense stellar winds (Wolf-Rayet stars) turn out to be fed mainly from recombination cascades. Consequently, the strength of those lines depends on the *square of* the density. Therefore, when clumping is accounted for, the main spectral features are (nearly) invariant if the mass-loss rate is diminished correspondingly such that $\sqrt{D}\dot{M} = constant$. In other words, all empirical mass-loss rates determined from the fit of such emission lines with un-clumped models are only upper limits. For deriving a definite $\dot{M}$, the value of D has to be known.

Fortunately there is a handle to determine the clumping contrast from detailed line fits. Photon scattering by free electrons ("Thomson scattering") is an important continuous opacity in hot stellar atmospheres. This process is by no means coherent, but redistributes the scattered photons over significant wavelength shifts due to the high thermal speed of the electrons. This effect leads to faint wings near the flanks of strong emission lines.

Now, electron scattering (as well as the P-Cygni shaped resonance lines) depend linearly on the density. Hence, with increasing density contrast D and

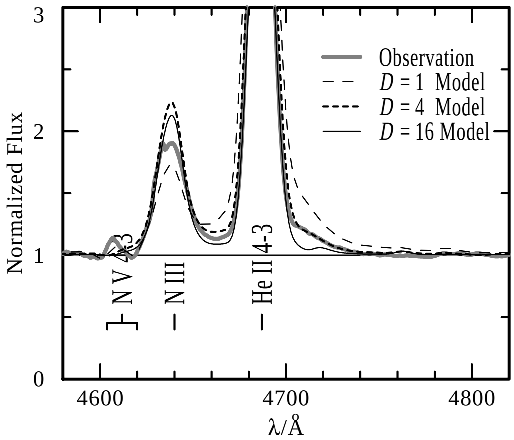

Figure 6. Model series with different clumping, compared to observation (WN7 star Br 24). An electron-scattering wing is visible especially at the red flank of the strong He II emission line at 4686 Å. Its strength depends on the clumping density contrast D. The mass-loss rate of the shown models is $\log\{\dot{M}/(M_\odot \mathrm{yr}^{-1})\}$ = -4.76, -5.06 and -5.36 for D = 1, 4, and 16, respectively (other parameters are as in Fig. 7). The observation is matched best with $D = 4$.

a compensating decrease of the mass-loss rate, the ρ^2-dependent emission lines keep their strength, while the electron-scattering line wings become weaker (cf. Fig. 6). Detailed profile fits for a few WR stars indicate $D = 4$ ... 10 as typical

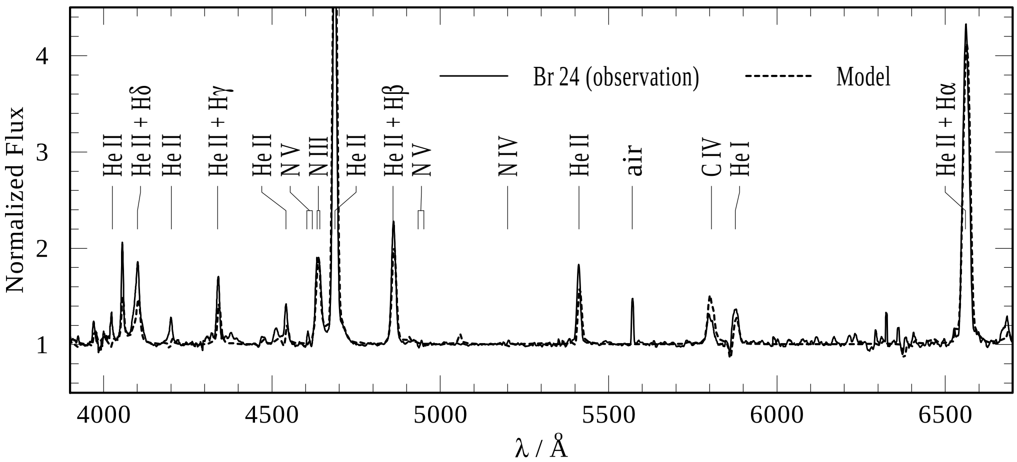

Figure 7. The observed visual spectrum of the WN7 star Br 24 in the LMC, compared to a model calculation with clumping ($D = 4$). Accounting for the clumping effect has nicely improved the detailed agreement between observed WR spectra and our models. Model parameters: $T_* = 40\,\mathrm{kK}$, $\log L/L_\odot = 5.35$, $\log \dot{M}/(M_\odot \mathrm{yr}^{-1})$ = -5.0, v_∞ = 950 km/s, composition H/He/C/N = 40/59/0.01/0.8 (by mass).

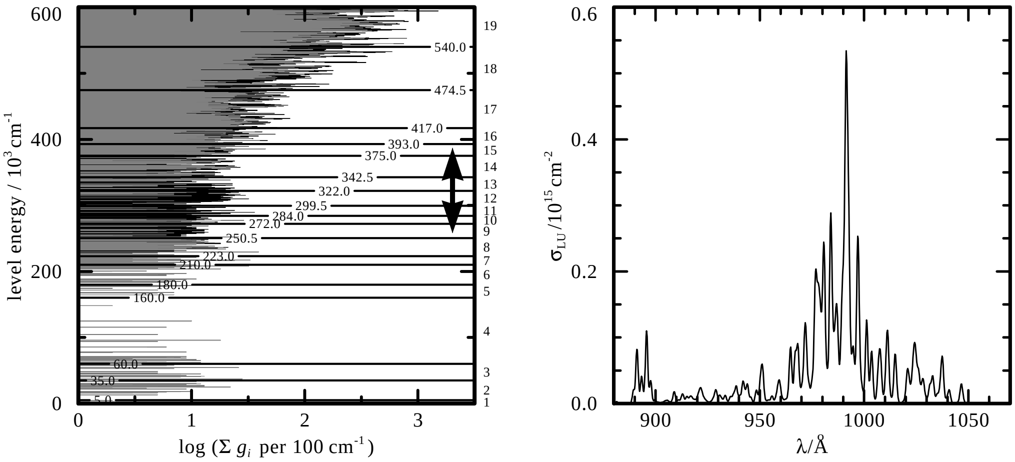

Figure 8. *Left panel*: Energy levels of ion V of our generic iron-group model atom (i.e. Fe V, Ni V etc.). Level energies are given in 10^3 Kayser (cm^{-1}). The statistical weights of the levels are plotted in bins of 100 Kayser. The contribution of levels with even parity is in grey. The 19804 levels of this model ion might be grouped into 19 superlevels as indicated. *Right panel*: Cross section of the superline between superlevels 9 and 15 (cf. left panel). The profile is composed of the numerous individual lines between the individual energy levels contained in the involved two superlevels.

values. Consequently, empirical mass-loss rates are scaled down by factors 2 ... 3, compared to previous estimates with smooth models.

1.7. Iron line blanketing in expanding atmospheres

The opacities of iron and iron-group elements are important for the atmospheres of hot stars. Often the observed spectrum in the UV is dominated by a "forest" of iron lines even forming a pseudo-continuum (see Fig. 8). Therefore the inclusion of "iron line blanketing" was a major progress towards a realistic modelling of expanding atmospheres (Hillier & Miller 1998, Gräfener et al. 2002).

The problem of treating iron and the other iron group elements (nickel etc.) in atmosphere models comes from the enormous complexity of their electron system. Present data collections comprise $\approx 10^5$ energy levels and $\approx 10^7$ line transitions between those levels.

A full non-LTE treatment of such model atoms is not possible. However, Anderson (1989) proposed the "superlevel concept" which allows an approximate treatment. Its basic idea is to group the numerous energy levels into a much smaller number (say, a few hundred) of "superlevels" for which non-LTE population numbers are calculated. Within each superlevel, the relative population of the individual levels is assumed to be in LTE (Fig. 8, left panel).

The radiative transitions between the superlevels form a "superline". Each superline is composed of all individual lines between the individual levels of the involved superlevels. Therefore the profile function covers a broad band with a complicated shape (Fig. 8, right panel).

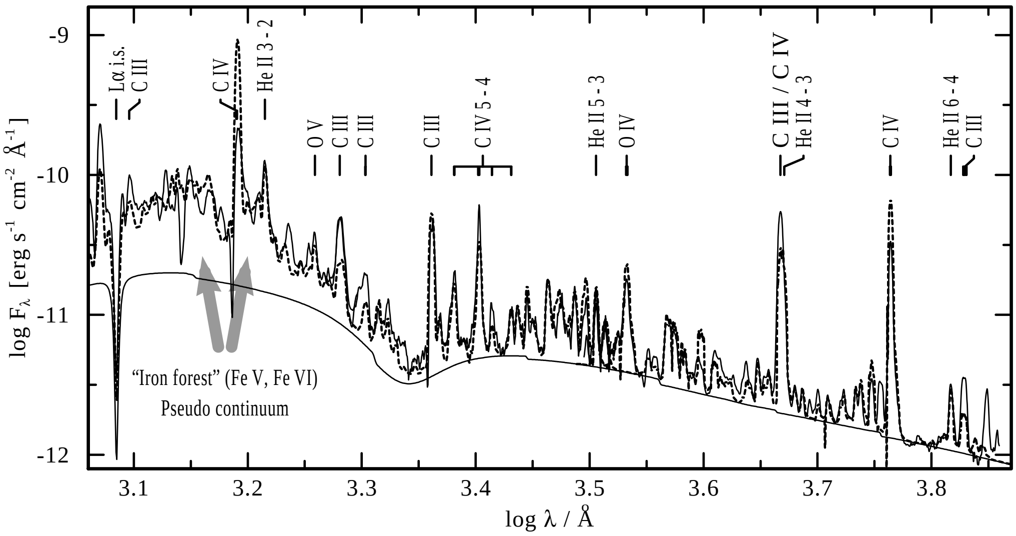

Figure 9. The observed calibrated spectrum of the galactic WC5 star WR 111 in the UV and visual (solid line), compared to a model calculation with clumping and blanketing (dashed line). The theoretical continuum is also shown for comparison (smooth solid line); the forest of iron lines forms a strong pseudo continuum in the UV. The model parameters are: $T_* = 141\,\mathrm{kK}$, $\log L/L_\odot = 5.68$, $\log \dot{M}/(M_\odot \mathrm{yr}^{-1}) =$ -4.8, $D = 10$, $v_\infty = 2000\,\mathrm{km\,s}^{-1}$, composition He/C/O = 55/40/05 (by mass), E_{b-v}=0.28 mag, $m - M = 11.09$ mag.

In static atmospheres there are techniques to simplify the radiative transfer for those complicated superline profiles. E.g., the frequencies might be rearranged according to the opacity and then represented by an "opacity distribution function (ODF). This cannot be applied in moving atmospheres, because each frequency point is coupled to its neighbors by Doppler shifts and therefore not relocatable. The only way out is to treat all these complicated superline profiles as they are, and resolve the individual lines with a sufficiently fine spacing of frequencies (typically 10^5 frequency points).

2. Modeling Wolf-Rayet atmospheres

2.1. The "Standard Model"

The so-called standard model for expanding atmospheres, which is applied for spectral analyses of hot stars with strong stellar winds (Wolf-Rayet stars, O stars, Central Stars of Planetary Nebulae ...), is based on the simplifying assumptions of spherical symmetry, stationarity and homogeneity (but allowing for small-scale clumping). The expansion velocity law is usually pre-specified by some analytical formulae with free parameters, and the density structure follows from the velocity law via the continuity equation. Radiative equilibrium determines the temperature stratification. Thus, a particular model atmosphere is specified by the following parameters: mass-loss rate $\dot{M}$, clumping contrast D, effective temperature T_* (related to the reference radius R_*, which we usually defined by $\tau_{\rm Rosseland} = 20$), luminosity $L = 4\pi R_*^2 \sigma T_*^4$, terminal wind velocity v_∞, and the chemical composition of the atmosphere.

2.2. Numerical implementation (Potsdam code)

Codes for expanding atmospheres have been developed independently by different groups (e.g. Hiller 1990, Hillier & Miller 1998). Here we briefly introduce the code written in Potsdam (formerly Kiel), most recently described by Gräfener et al. (2002).

The radiation transfer is solved in the Co-Moving Frame (CMF), using the differencing scheme for the moment equations. The Eddington factors are updated every six iterations by solving the angle-dependent radiation transfer with Short Characteristics integration.

Diagonal ALOs are used to incorporate an approximate radiation transfer into the non-LTE statistical equilibrium equations, which therefore (and because of using "net radiative brackets") become non-linear. This system is solved iteratively by Broyden's method (Koesterke et al. 1992).

Complex model atoms of H, He, H, C, N, O ... are (optionally) implemented. Iron line blanketing is accounted for by grouping the numerous energy levels into 10 – 20 superlevels per ion. The iron-group elements (Fe, Ni, Co, Ti ...) are compounded to one "generic atom". In total, we treat typically 300 non-LTE levels and a few thousand lines.

Radiative equilibrium is achieved by a kind of Unsöld-Lucy temperature correction method, adapted to the spherically expanding case. The convergence is speeded up by incorporating an approximate lambda operator into the energy balance. – The emergent spectrum is finally calculated in the observer's frame.

2.3. Towards hydrodynamical wind models for Wolf-Rayet stars

The line-blanketed non-LTE models allow to evaluate the radiation pressure exerted on the matter. Without relying on crude approximations, all complex mechanisms like multiple scattering are automatically included. If those calculations could be combined with the hydrodynamical equations, the velocity field and mass-loss rate could be calculated self-consistently (cf. Gräfener, these proceedings).

Self-consistent models already exist, with more or less approximate treatment of the non-LTE radiation transfer, for the relatively thin winds from OB stars. However, the much stronger mass-loss from Wolf-Rayet stars can not yet be explained. As a first step to understand the special effects acting in WR-type winds, we study the radiative force provided by our models.

For that purpose, we calculate a grid WR model atmospheres with an adopted (i.e. inconsistent) velocity law. For series with different effective temperatures, $\dot{M}$ is varied while all other parameters are kept fixed ($\log L/L_\odot = 5.3$, $v_\infty = 2000\,{\rm km\,s^{-1}}$, $D = 10$, He/C/O/Fe = 55/40/5/0.16). For each model we integrate the work done by the radiative force, $\int f_{\rm rad}\,{\rm d}r$, and compare this with the work actually needed to accelerate the wind. (In a consistent model, this "work ratio" Q should be unity. The remaining shortfall might be attributed to still incomplete opacities.)

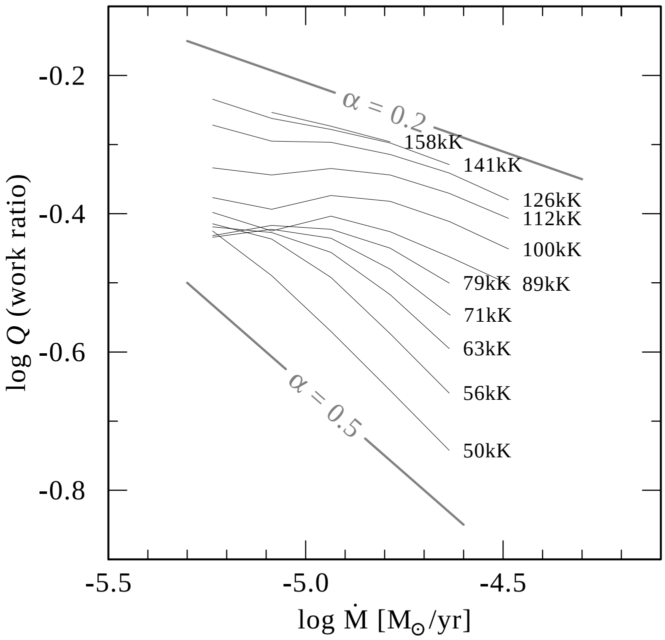

Figure 10. "Work ratio" Q (see text) for series of WC models with different effective temperature T_* (labels). The dependence of Q on $\dot{M}$ reflects the exponent α of the CAK theory.

In the framework of the radiation-driven wind theory by Castor, Abbott, & Klein (1975), Q should scale with $\dot{M}^{-\alpha}$ where the parameter α reflects the relative contribution from optically thick lines to the radiative force. In O star models, always $\alpha \approx 0.7$ is found. The much shallower slope seen in Fig. 10 ($\alpha =$ 0.2 ... 0.5) shows that WR winds are mainly driven by weak lines and continua.

References

Anderson L.S. 1989, ApJ 339,558

Castor J.I., Abbott D.C., Klein R.I., 1975, ApJ 195, 157

Gräfener G., Koesterke L., Hamann W.-R. 2002, A&A 387, 244

Hamann W.-R. 1985, A&A 148, 364

Hamann W.-R. 1986, A&A 160, 347

Hillier D.J., 1990, A&A 231, 111

Hillier D.J., Miller D.L. 1998, ApJ 496, 407

Koesterke L., Hamann W.-R., Kosmol P. 1992, A&A 255, 490

Koesterke L., Hamann W.-R., Gräfener G.. 2002, A&A 384, 562

Mihalas D., Kunasz P.B., Hummer D.G. 1975, ApJ 202, 465

Mihalas D., Kunasz P.B., Hummer D.G. 1976, ApJ 210, 419

Olson, G.L., Auer, L.H., Buchler, J.R. 1986, JQSRT 35, 431

Werner K., Husfeld D. 1985, A&A 148, 417